ACS Combinatorial Science

Research Article

pubs.acs.org/acscombsci

High-Throughput Measurements of Thermochromic Behavior in $V_{1-x}Nb_xO_2$ Combinatorial Thin Film Libraries

S. C. Barron,* J. M. Gorham, M. P. Patel, and M. L. Green

Material Measurement Laboratory, National Institute of Standards and Technology, 100 Bureau Drive, MS 8520, Gaithersburg, Maryland 20899-8520, United States

Web-Enhanced Feature

ABSTRACT: We describe a high-throughput characterization of near-infrared thermochromism in $V_{1-x}Nb_xO_2$ combinatorial thin film libraries. The oxide thin film library was prepared with a VO_2 crystal structure and a continuous gradient in composition with Nb concentrations in the range of less than 1% to 45%. The thermochromic phase transition from monoclinic to tetragonal was characterized by the accompanying change in near-infrared reflectance. With increasing Nb substitution, the transition temperature was depressed from 65 to 35 °C, as desirable for smart window applications. However, the magnitude of the reflectance change across the thermochromic transition was also reduced with increasing Nb film content. Data collection, handling, and analysis supporting thermochromic characterization were fully automated to achieve high throughput. Using this system, in 14 h, temperature-dependent infrared reflectances were measured at 165 arbitrary locations on a thin film combinatorial library; these measurements were analyzed for thermochromic transitions in minutes.

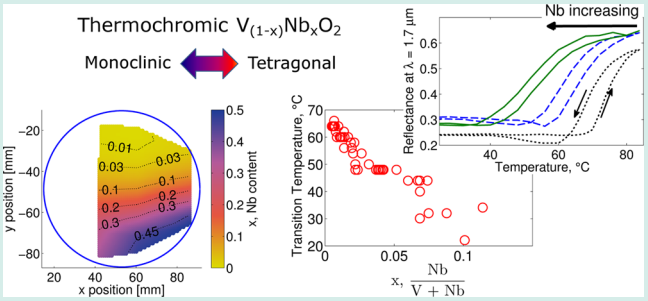

KEYWORDS: *high-throughput screening, thermochromics, combinatorial thin film library, near-infrared reflectance, metal−insulator transition, vanadium dioxide (VO_2)*

INTRODUCTION

In 2010 half of the 39×10^{15} BTUs (41×10^{18} J) consumed by U.S. residential and commercial buildings were used to maintain lighting, heating, and cooling systems.[1] The implementation of smart window technologies that modulate the transmittance of solar radiation has the potential to dramatically decrease such energy use, and there is active research into the engineering challenges of appropriate building design and fenestration, control systems, and materials.[2−6]

The materials under investigation include those whose optical properties in the visible or near-infrared (NIR) parts of the solar spectrum can change in response to either temperature (thermochromic materials) or electrical potential (electrochromic materials). While windows based on electrochromic materials are more developed, they require external power systems and multilayer coatings to integrate the transparent electrodes.[4,8] This paper focuses on thermochromic materials, which offer a simpler window design and require no control or power systems; rather, the change occurs in response to variations in the ambient temperature, since the window coating undergoes a transition from a low temperature, NIR transparent state when solar heating is desirable, to a high temperature NIR reflective state when it is undesirable.

For smart window applications, the thermochromic transition should take place within the range of ambient temperatures on the Earth's surface. A transition temperature of less than 25 °C offers the greatest savings in energy consumption,[6,7] but windows with higher transition temperatures also provide energy savings, since the thermochromic layer, embedded in the window, may reach temperatures in excess of 45 °C on particularly warm, sunny days.[5,8] Vanadium dioxide exhibits the desired transition in NIR optical properties but at too high a temperature,[6,9−11] a result of the insulator to metal transition it undergoes at 68 °C.[12−15] Substitutional impurities, such as W, Nb, and Mo, have been found to depress the VO_2 transition temperature in bulk, thin film, and nanostructured samples,[16−23] while dopants such as Mg can additionally increase visible transmittance,[24,25] but the disparities in material preparation and sample dimensions make comparisons across studies difficult.

These concerns can be addressed by analysis of combinatorial libraries, in which film composition varies continuously across the sample.[26−34] These combinatorial libraries, prepared in specially designed chemical or physical vapor deposition systems (CVD or PVD), have the advantages of rapidly generating many film compositions, thus mitigating many sample-to-sample variations,[29−35] and are particularly valuable in the study of electronic or crystallographic phase transitions in which properties can change dramatically.[29,35−37] Further, there are only a few systematic studies of multiply doped VO_2;[20,38]

Received: April 21, 2014
Revised: July 17, 2014
Published: September 2, 2014

such ternary and higher-order oxide compositions can be readily produced by combinatorial thin film syntheses.

In this paper, we describe a high-throughput, combinatorial methodology for characterizing thermochromism in $V_{1-x}M_xO_2$ thin films with a continuous composition gradient. This study uses the particular case of M = Nb as a model system, since Nb is an impurity that has been shown to depress the transition temperature with moderate efficiency.[16,21,22,39] However, the metrology described is appropriate for any impurity that can be deposited by pulsed laser deposition (PLD) from a solid target, and future studies using this system may focus on the high-throughput discovery of substitutional impurities with more efficient depression of the transition temperature, similar to W.

METHODS

Thin film samples were prepared by PLD from ceramic targets. Some samples were prepared as combinatorial thin film libraries in a method described previously for our system.[40−43] In this technique, a continuous gradient in film composition resulted from the combined effects of the natural spatial nonuniformity of the deposition plume emitted from a given target, and the positioning of chemically distinct targets. In this study, the targets were 25.4 mm disks of V_2O_5 (Kurt J. Lesker, Pittsburgh, PA) and Nb_2O_5 (Plasmaterials, Livermore, CA).

A KrF laser (wavelength = 248 nm) was pulsed at 10 Hz with energies of 200−230 mJ/pulse. For the VO_2 film, the total number of pulses to the V_2O_5 target was 160 000 for a maximum film thickness of 297 nm. For the $V_{1-x}Nb_xO_2$ combinatorial thin film libraries, the laser alternated between the targets in a ratio of 100 pulses V_2O_5 for every 15 pulses to the Nb_2O_5, for a total of 92,000 pulses. On the substrate, the distance between the center of VO_2 deposition and the center of the Nb oxide deposition was approximately 48 mm, due to a substrate rotation of 120° between targeting each metal oxide. During deposition the oxygen partial pressure was 0.65 Pa, which had previously been found to result in VO_2 films from V_2O_5 targets.[40] Thin films were deposited on 76.2 mm diameter silicon substrates, which were radiatively heated to 520 °C. While the temperature recorded off the heater thermocouple during film deposition was significantly higher (approximately 200 °C greater), the corresponding substrate surface temperature was estimated based on previous measurements of a thermocouple pasted to the surface of a blank substrate during heating in vacuum; the estimated uncertainty was ±30 °C. After deposition, the sample was allowed to cool to room temperature in vacuum.

Crystalline phase structure was characterized by X-ray diffraction in a Bruker D8. The X-ray source was Cu Kα radiation and the spot size was approximately 1 mm × 2 mm. The instrument was equipped with an area detector, and a sample stage that allowed 80 mm translation in two directions for automated data collection, which was in a serpentine pattern of measurement spots spaced at 5 mm across the entire library film.

To generate a map of the elemental distribution across the $V_{1-x}Nb_xO_2$ combinatorial library wafer, X-ray photoelectron spectroscopy (XPS) was carried out on three sections cut from the library wafer. To aid in aligning analysis locations among the sections, the uncut wafer had a physical mark scribed across the wafer diameter as a observable point of reference. XPS spectra were acquired on a Kratos Axis Ultra DLD spectrometer (Kratos Analytical, LTD; Chestnut Ridge, NY) using monochromatic Al Kα X-rays operating at 150 W under ultra-high vacuum (UHV) conditions ($P_{base} < 10^{-7}$ Pa). Emitted photoelectrons were collected along the surface normal using a hybrid lens and slot aperture with 90% of the signal collected from a 0.94 mm × 2.25 mm area. Analysis areas were uniformly spaced every 4.0 mm along the length of each library section. The collected photoelectrons were analyzed and displayed as high resolution spectra at 0.1 eV steps using a pass energy of 20 eV and a dwell time of 500 ms per step. The Nb (3d) spectra were acquired over 6 sweeps per analysis point while the V (2p) spectra were acquired over 4 sweeps.

Analysis of the spectra after acquisition was performed using CasaXPS (CasaXPS LTD; Teignmouth, UK). All spectra were analyzed without energy adjustment and were fitted with a Shirley background. For Nb ($3d^{5/2} \approx 206.7$ eV), the elemental composition was determined from the area under the curve after background subtraction. However, because of the proximity of the V peak (V $2p^{3/2} \approx 517.2$ eV; $2p_{1/2} \approx 524.7$ eV) to the O peak (O 1s ≈ 530 eV), the spectral area of the V was determined through fitting the region to 2 distinct vanadium oxide species (4 peaks) and 2 distinct oxygen chemical species (2 peaks). All peaks were 70% Lorentzian/30% Gaussian with the only constraint on the fits being the loose peak locations and setting V $(2p^{1/2}) = 0.5 \times$ V $(2p^{3/2})$. After summing up the areas and the errors of the fits, percent compositions were calculated using Kratos-derived elemental relative sensitivity factors (RSF) of 2.921 and 2.116 for the Nb (3d) region and V (2p) regions, respectively. All reported values reflect the percent atomic surface concentration based on analysis of only the V and Nb peaks. Error bars represent the standard deviation associated with the background (Nb) or the quality of the fit (V).

Film thicknesses are reported based on visible light spectroscopic reflectometry in normal incidence.[42] The complex indices of refraction were derived from spectroscopic ellipsometry for a VO_2 film deposited on silicon at 200 °C.

A high-throughput measurement tool has been designed and constructed for the automated collection of NIR reflectance spectra at numerous arbitrary locations across the library films at temperatures between 15 and 85 °C. The sample temperature was regulated by a thermoelectric heater/cooler (TECMount, Arroyo Instruments, San Luis Obispo, CA) with a 90 mm × 90 mm plate. Once the temperature was stable, the thermoelectric heater/cooler was translated on a 100 mm x-y stage below a stationary reflectance probe. The NIR reflectance was measured in normal incidence, using a fiber optic coupled spectrometer (NIRQuest256−2.5, Ocean Optics, Dunedin, FL) employing an InGaAs detector sensitive to wavelengths between 0.9 and 2.5 μm. The raw reflected intensity was normalized to the reflected intensity from a 100 nm Au film electron beam deposited on a silicon wafer. The three instrument controllers were automated via a custom-built LabVIEW program.

For the library sample reported here, reflectance spectra were taken at 17 temperatures on heating and again on cooling (35 temperature steps total). At each measurement temperature, 165 different locations were measured at 5 mm spacings across the 76.2 mm wafer, each representing a unique film composition. In this way, 5775 reflectance spectra were collected in 14 h.

The metrology described here was focused on high-throughput identification of materials with appropriate transition temperatures for smart windows and relied on high-throughput NIR reflectance measurements from thin films

dx.doi.org/10.1021/co500064p | ACS Comb. Sci. 2014, 16, 526−534

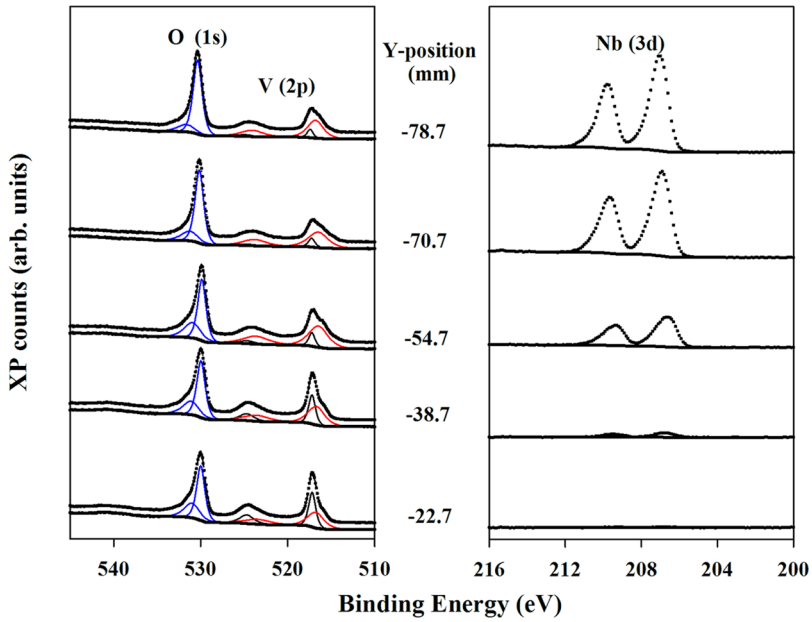

Figure 1. Fitted XP spectra of the Nb-substituted VO_2 from select positions along the *y*-axis of the library film (*x*-position = 60 mm). (Left) V (2p) and the O (1s) spectral features were fitted to deconvolute the spectra. The raw data and the composite fit are offset for ease of viewing. (Right) The Nb (3d) region was fit with a background and the area under the curve was acquired.

deposited on silicon wafers. Thermochromism in VO_2 films has often previously been reported from measurements of transmission and sometimes, reflectance from films deposited on transparent substrates.[16,18,21,22,35,44] These transmission measurements are ultimately necessary to characterize luminous transmission and solar energy modulation for evaluating smart window coatings. To develop the high-throughput measurement technique described here, however, optical access was limited to one side of the sample, resulting in a reflection measurement only; the sample heater blocked access to the backside of the wafer.

We note that the silicon wafer on which the $V_{1-x}Nb_xO_2$ thin films were deposited has some infrared transparency, and hence, the reflectances reported here are characteristic of the (film + substrate) ensemble and cannot simply be attributed to the film.

To present our data, we represent each reflectance spectrum by the reflectance value at a single wavelength, 1.7 μm, chosen because it is representative of the NIR solar radiation reaching the Earth's surface (i.e., not absorbed in the atmosphere)[45] and is not blocked by the soda lime glass used for most building windows.[46] However, we will show that there are no abrupt changes with wavelength in the reflectance spectra, and so the choice of representative wavelength is somewhat arbitrary. To quantify the transition temperatures for each film location in an automated way, we plot the reflectance at 1.7 μm versus temperature and take the numerical derivative of the hysteresis curve. The transition temperature was defined as the average of the temperatures with the maximum derivative on heating and cooling, and the hysteresis width as the difference between these temperatures. This data reduction algorithm was implemented in a MATLAB script to process data after collection.

LIBRARY CHARACTERIZATION

First, we describe the composition variation across the $V_{1-x}Nb_xO_2$ library, focusing on the lateral distribution of transition metals. Figure 1 presents select V (2p) and Nb (3d) spectra taken across the central strip of the library. As Figure 1 clearly demonstrates, the V (2p) region decreased in photoelectron intensity while the Nb (3d) feature increased as the *y*-position decreased.

Though the focus was on accurately calculating *elemental* distributions as opposed to the *chemical* distributions of the transition metals, we can infer based on the V ($2p^{3/2}$) peak positions that one species at (517.2 ± 0.1) eV is likely representative of V^{5+} and the second species at (516.6 ± 0.2) eV is comparable to V^{4+}.[22,47] (Peak positions are based on the average and SD of 42 separately fitted spectra). This is in contrast with the Nb (3d) spectra (Figure 1, right) which appeared to consist of one chemical species. Indeed, the Nb ($3d^{5/2}$) peak was located at (206.7 ± 0.1) eV, comparable to oxidized niobium.[48] In addition to the metal oxides, the only other elements detected were carbon and nitrogen which were attributed to surface contamination.

The compositional change is more readily apparent in Figure 2a, which plots the V (2p) surface content along the same central strip (located at an x position of 60 mm). The V (2p) content is denoted as $(1 - x)$ according to the chemical formula $V_{1-x}Nb_xO_2$. The film is predominantly V oxide across the entire sample strip, with the $(1 - x)$ V content ranging from (51.9 ± 2.1) % to (99.6 ± 0.3) %. Between the extremes, the V surface content increased with increasing y-position and followed a sigmoidal trend. In Figure 2b, the V content is plotted for all 3 strips of the $V_{1-x}Nb_xO_2$ library.

As our goal was to map thermochromic behavior as a function of film composition, it is useful to compare the spatial resolution of the thermochromic measurement to the compositions represented on the $V_{1-x}Nb_xO_2$ library and to the concentration gradient. From previous studies,[16,21,22,39] the desired thermochromic temperature is likely to occur at $x < 0.1$ Nb substitution. From Figure 2, the desired composition range covered ~40% of this library film with gradient in Nb content *x* of <0.008/mm. Hence, the composition range of interest was

dx.doi.org/10.1021/co500064p | ACS Comb. Sci. 2014, 16, 526−534

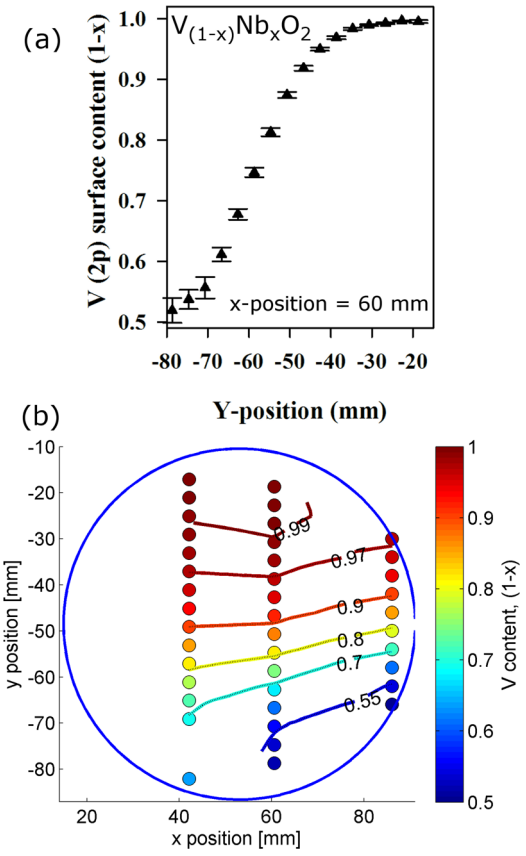

Figure 2. XPS measurements of the cation distribution of $V_{1-x}Nb_xO_2$ thin film library. (a) Vanadium surface content $(1 - x)$ measured at 4.0 mm intervals along the *y*-axis. Each value is representative of 1 measurement ±1 standard deviation of the fits. (b) Vanadium surface content $(1 - x)$ as a function of position on the full combinatorial library. Spots are locations of XPS measurements. Contour lines $(1 - x)$ are a smooth interpolation among XPS measurements. The circle represents the extent of the library film, deposited on a 76.2 mm diameter substrate.

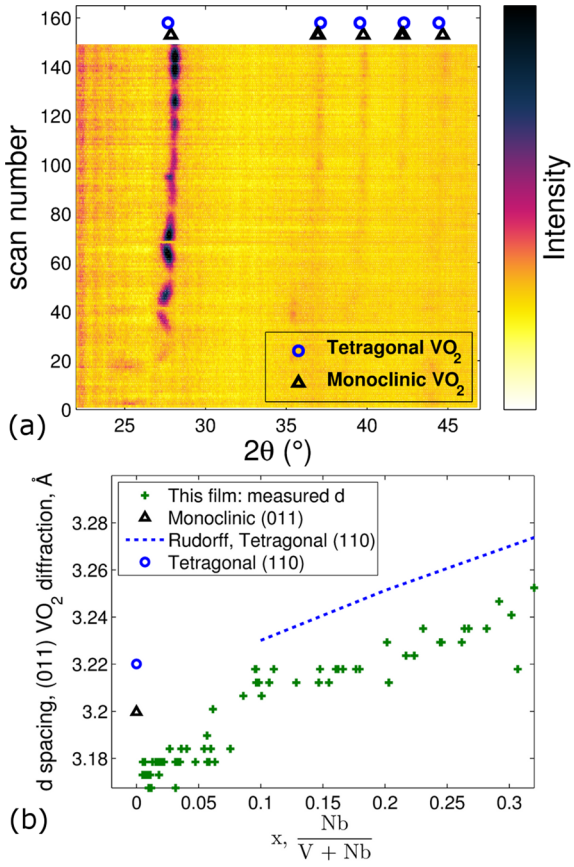

Figure 3. (a) X-ray diffraction patterns from 149 locations on the $V_{1-x}Nb_xO_2$ thin film library. Diffraction is expected from monoclinic (▲) and tetragonal (○) VO_2 phases at the marked 2θ from JCPDS 44-252 and 44-253, respectively. The regions of the film with the greatest Nb content are at the lower scan numbers. (b) The *d*-spacing associated with diffraction from the monoclinic (011) planes or tetragonal (110) planes increased with increasing Nb content. Rudorff is ref 46.

mapped with a high density of thermochromic measurement spots, assuring that many similar concentrations were measured. Further, within this range, the average change in composition, Δx, across a single measurement spot (1 mm diameter) was less than 0.008. Steeper concentration gradients, up to 0.02/mm, were present at Nb contents (x = 0.3 Nb, for example) that were of less interest because they did not exhibit a thermochromic phase transition.

The surface oxygen content was not analyzed quantitatively from the XPS results, since the focus was on the V:Nb cation ratio and surface oxygen concentration was likely different than the film bulk. The X-ray diffraction patterns and thermochromic behavior exhibited by the film bulk were characteristic of VO_2, and so the film composition is presented here in the form of $V_{1-x}Nb_xO_2$.

Figure 3a displays X-ray diffraction spectra for 149 locations on the $V_{1-x}Nb_xO_2$ thin film library, with intensity indicated by color. The first scan collected was in the most Nb-rich region of the library; collection continued in a serpentine pattern toward the V-rich region. Diffraction from monoclinic and tetragonal VO_2 phases is expected at the marked 2θ values. Because diffraction from the two phases differ mostly in peak splitting and shifting and because Nb substitution also results in peak shifts, we can conclude only that 80% of the library film exhibited diffraction powder patterns consistent with the presence of crystalline VO_2. No other crystalline phases were apparent in any of the scans, and the most Nb-rich regions of the film were amorphous or poorly crystalline.

In Figure 3b, the *d*-spacing of the strongest VO_2 diffraction at $2\theta \approx 28°$ is plotted as a function of Nb content. The planes giving rise to this diffraction are the (110) planes in the high temperature tetragonal structure; in the low temperature distortion to the monoclinic crystal structure, these same (distorted) planes are referred to as (011) planes. The *d*-spacings for the most pure VO_2 in this library were somewhat lower than that expected of monoclinic or tetragonal phase. The *d*-spacing increased from 3.17 Å for the most pure VO_2 to 3.25 Å for a film concentration of x = 30% Nb, consistent with the incorporation of the larger Nb atoms into the VO_2 crystalline lattice and similar to the trend observed for a series of bulk $V_{1-x}Nb_xO_2$ in the tetragonal rutile structure.[49] Some of the Nb could also have segregated to grain boundaries or precipitated as a minor phase. We have not attempted to distinguish these possibilities by XPS, but the continued increase in VO_2 *d*-spacing even at the highest Nb contents indicated any secondary phase was a low volume fraction. Largely, the crystalline phase structure of 80% of the library film

dx.doi.org/10.1021/co500064p | ACS Comb. Sci. 2014, 16, 526−534

was a continuous solid solution of Nb substitution into the VO_2 crystalline lattice.

RESULTS AND DISCUSSION

Combinatorial experiments require both automating the collection of large quantities of data and then automating the necessary data reduction to make useful conclusions. In this section, we first describe the collection of high quality thermochromic spectral reflectance data comparable to many noncombinatorial experiments. Second, we utilize a robust data handling protocol for data visualization and reduction that realizes the high throughput paradigm of combinatorial research.

Thermochromic Spectral Reflectance from VO_2 and Nb-Substituted VO_2. Figure 4a displays the infrared reflectance of a VO_2 thin film of 293 nm thickness at selected temperatures as the sample was heated from 20 to 80 °C. As measurement temperature increased, the infrared reflectance increased, indicative of the expected phase transition from the NIR transparent monoclinic phase to the NIR reflective tetragonal phase. Most of the increase in reflectance during heating occurred between 68 and 76 °C.

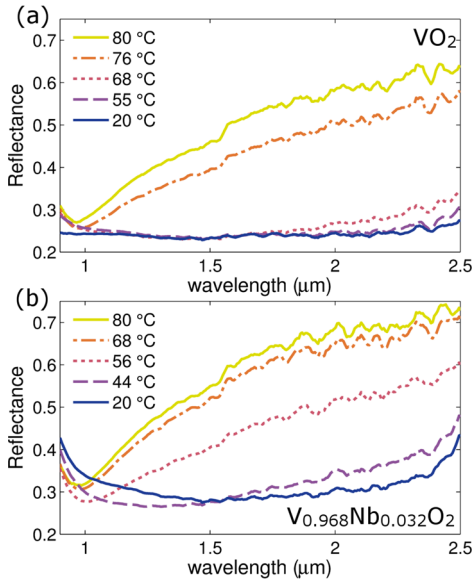

Figure 4. NIR reflectance at several temperatures (a) from VO_2 film and (b) from a region of the $V_{1-x}Nb_xO_2$ combinatorial library with x = 3.2% Nb. Note that the temperatures on panels a and b are different.

In Figure 4b, we plot similar reflectance spectra for a region of the $V_{1-x}Nb_xO_2$ combinatorial library with x = 3.2% Nb and a thickness of 190 nm. (Note that some of the temperatures chosen for this plot are different from those in Figure 4a.) With low levels of Nb substitution, the thermochromic transition occurred at lower temperatures. For this sample, much of the NIR reflectance increase occurred between 44 and 56 °C, with further increases at 68 °C.

While the shape of the reflectance spectra at high temperatures was very similar to that of the VO_2 film, it appears that the low temperature reflectance of the Nb-substituted film diverged for wavelengths less than 1.4 μm. This could be due to a localized Nb impurity state, but we have not investigated this effect further.

In the next section, we describe the data reduction made in extracting useful parameters (i.e., those indicative of the thermochromic transition). The full spectral reflectance was retained, however, and could be mined for other trends such as reflectance at lower wavelengths, as becomes relevant.

High-Throughput Analysis of Thermochromic Behavior in a $V_{1-x}Nb_xO_2$ Combinatorial Library. We now further characterize the effect of Nb-substitution on the thermochromic VO_2 phase transition, utilizing high-throughput measurements and analysis of a combinatorial $V_{1-x}Nb_xO_2$ thin film library. The previous section discussed measurements made on this library, but only at a single location, that is, at a Nb content of 3.2%, and only at five temperatures on heating. The reflectance spectra in Figure 4b are a small subset of the 5775 spectra collected for 165 unique film compositions on the thin film library. In this section, the full composition space represented is discussed.

For high-throughput data visualization and plotting, it is desirable to represent each reflectance spectra by a single value. Here, we choose to extract the reflectance at 1.7 μm, a wavelength at which there is significant variation as a result of the phase change. Other researchers have used the transmission at 2[35,44] or 2.5[18−22] μm in similar analyses. Of importance to smart window applications, all three of these wavelengths can pass through the soda lime glass (transparent up to about 3 μm) of most building windows.[46] To utilize the full

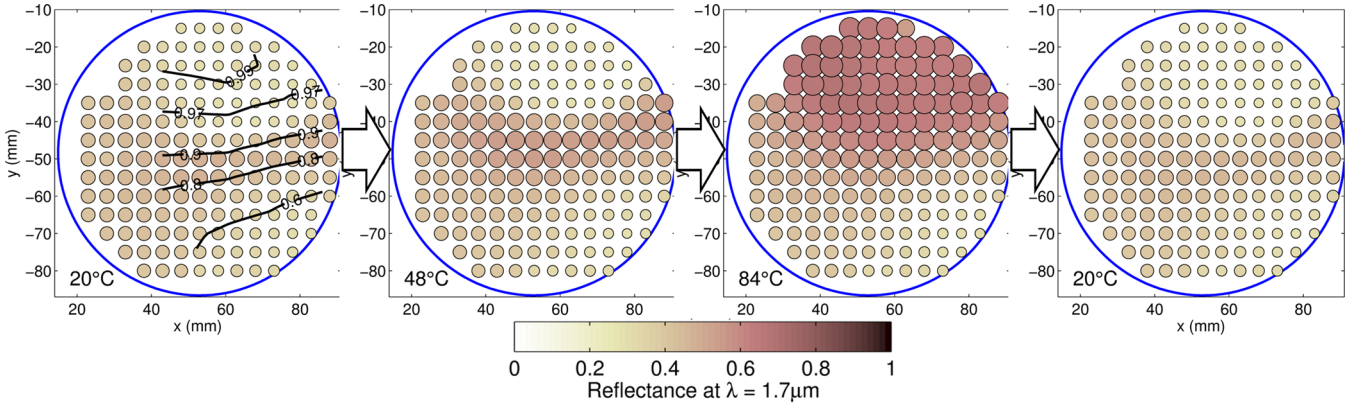

Figure 5. NIR reflectance is mapped as a function of position on the 76.2 mm diameter $V_{1-x}Nb_xO_2$ combinatorial library at selected temperatures, as the sample is heated from 20 to 84 °C, and then cooled back to 20 °C. The vanadium content $(1 - x)$ is marked on the first 20 °C map. An animation of all 35 temperatures probed in this experiment is available online.

dx.doi.org/10.1021/co500064p | ACS Comb. Sci. 2014, 16, 526−534

transmission spectrum, some works[24,25] have computed the solar energy modulation based on the material's transmission and the wavelength-integrated weighting of the solar irradiance for air mass 1.5 (ref 45). Though this study did not measure materials in transmission and hence did not characterize solar energy modulation, we can use the wavelength-integrated solar irradiance to compare the three wavelengths. In terms of solar irradiance, there is more than twice as much radiation at 1.7 μm than at 2.0 μm, and essentially no 2.5 μm radiation since it is absorbed by water in the atmosphere.[45] However, the reflectance spectra in Figure 4 had no abrupt changes or features in this wavelength range and so transition temperatures derived from any of these three wavelengths should be comparable.

In Figure 5, we map the reflectance at 1.7 μm at 165 measurement locations across the 76.2 mm diameter $V_{1-x}Nb_xO_2$ library, at selected temperatures on heating and cooling. An animation of all 35 temperature steps this library experienced on heating and cooling is available online as Supporting Information. The level of reflectance is indicated by the size of the marker and its color according to the color bar, and the measurement temperature for each map is marked in the lower left. On the first 20 °C map, contours indicating the V content are marked.

We find that by 48 °C, the locations on the library with x = 5−15% Nb (i.e., 0.95−0.85 V) were exhibiting high NIR reflectance, indicative of the high temperature rutile phase, while the more pure VO_2 remained in the low temperature, low reflectance phase. By 80 °C, 50 percent of the library sample was in the high temperature phase, as indicated by its high reflectance. The transition was reversible, with the reflectances returning to their low values when the library sample was cooled to 20 °C.

The reflectance in regions of the $V_{1-x}Nb_xO_2$ library with the highest Nb content (x > 0.2) did not change with temperature. In parts of this region, there was no VO_2 crystalline phase, as determined by X-ray diffraction (Figure 3a). There was also a region of the library, with a composition of x = 0.2 to x = 0.35, that exhibited VO_2 diffraction but no thermochromism. This could be because significant oxygen vacancies or disorder existed in this thin, high Nb content region. The absence of thermochromic behavior in these parts of the film acted as a check on our measurement system, eliminating the possibility that the increased reflectance was a result of greater emittance from a hotter substrate. Rather, it appeared that increased temperature from 20 to 80 °C had essentially no effect on the radiation emitted from a film that did not undergo a phase change; this result has further been confirmed by making similar measurements on a bare silicon wafer.

In Figure 6, we plot the NIR reflectance at 1.7 μm as a function of measurement temperature for four different locations (compositions) on the $V_{1-x}Nb_xO_2$ library and for the VO_2 film of Figure 4a. Averaging over all measurements on the VO_2 film, the transition temperature was 69.3 ± 1.7 °C, with a hysteresis of 6.5 ± 3.9 °C, identical to the 68 °C expected for bulk and thin film VO_2.[12−14,50] The transition temperature decreased with increasing Nb content, reaching as low as 20−30 °C for 8.8% Nb. For this composition, however, the transition temperature was ill-defined since the reflectance was still changing at the lowest measurement temperature. At even greater Nb contents (x = 0.229), there was little to no reflectance change with temperature; rather the reflectance remained constant at an intermediate value between that of the high temperature and low temperatures phases of other compositions.

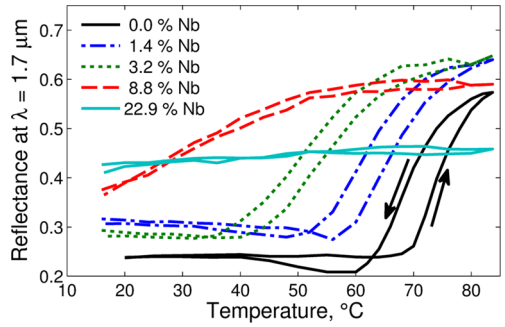

Figure 6. Reflectance for a wavelength of 1.7 μm as a function of temperature for a pure VO_2 film (0% Nb) and at a few library locations on $V_{1-x}Nb_xO_2$ combinatorial sample (varying Nb contents).

For the three samples with the lowest Nb content, there was discernible thermal hysteresis, with higher transition temperatures on heating than on cooling. The hysteresis was less than 10 °C, comparable to or lower than polycrystalline thin films reported elsewhere.[19,21,22,39] The lowest hysteresis was for the highest Nb content shown that exhibits thermochromism, x = 8.8% Nb, but for this composition the transition occurred over a greater range of temperatures. Further, the high temperature reflectance was not as a high as the high temperature reflectances of the film regions that have lower Nb content. In fact, across the library film, there was a continuous change in thermochromic behavior between the gradual switching at 8.8% Nb to the absence of switching at 22.9% Nb. Again, this may be indicative of regions of the film with a significant volume fraction of material without the VO_2 crystal structure, for example a dual phase region of crystalline Nb-substituted VO_2 and an amorphous mixed V−Nb oxide. Alternatively, it is also possible that either the tetragonal rutile phase or a metastable intermediate or disordered phase was stabilized.[51,52]

In Figure 7, for different Nb contents, we plot the maximum reflectance (at high temperatures) and minimum reflectance (at low temperatures) of each measurement spot on the library. The difference in reflectances was greatest for the lowest Nb content and decreased with increasing Nb content. While some of this apparent decrease can be attributed to not capturing the minimum reflectance at the lowest measurement temperature (8.8% Nb in Figure 6, e.g.), the maximum reflectance was also substantially reduced. For Nb substitutions greater than 15%,

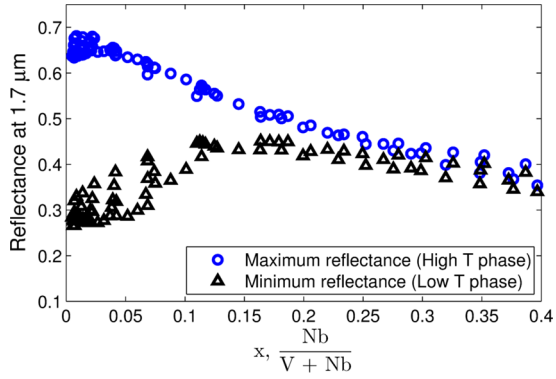

Figure 7. Maximum and minimum reflectances of each measurement location vs Nb content in a $V_{1-x}Nb_xO_2$ combinatorial library.

dx.doi.org/10.1021/co500064p | ACS Comb. Sci. 2014, 16, 526−534

there was essentially no thermochromism exhibited, as is also evident in Figure 6.

The effect of Nb substitution in VO_2 was similar to that described by previous researchers: substitution with transition metals, such as Nb and W, depresses the VO_2 transition temperature but also reduces the difference in resistivity and reflectivity between the two phases.[16,18−21,39,51,53−55] Increasing Nb content beyond $x = 0.05$ results in a transition that occurs more gradually over a broad range of temperatures.[39,53] Dopants have also been found to reduce the thermal hysteresis of the phase transition.[20]

In comparing Figures 6 and 7 to the structural information in Figure 3, we find that the highest Nb content at which any thermochromic transition occurred was in the range of x = 0.1−0.15. At the low end of this range, in Figure 3b, $x = 0.1$ also saw an abrupt increase in d-spacing of the VO_2 crystalline phase. This may indicate the necessary Nb content to transition to the tetragonal rutile phase at room temperature or to stabilize a metastable state with no thermochromic transition. A similar limit ($x = 0.1$) was found for suppressing metal−insulator phase transitions in bulk Nb-substituted VO_2 pellets.[51,53]

In Figure 8, we plot the thermochromic transition temperature as a function of the Nb content for the regions of the film

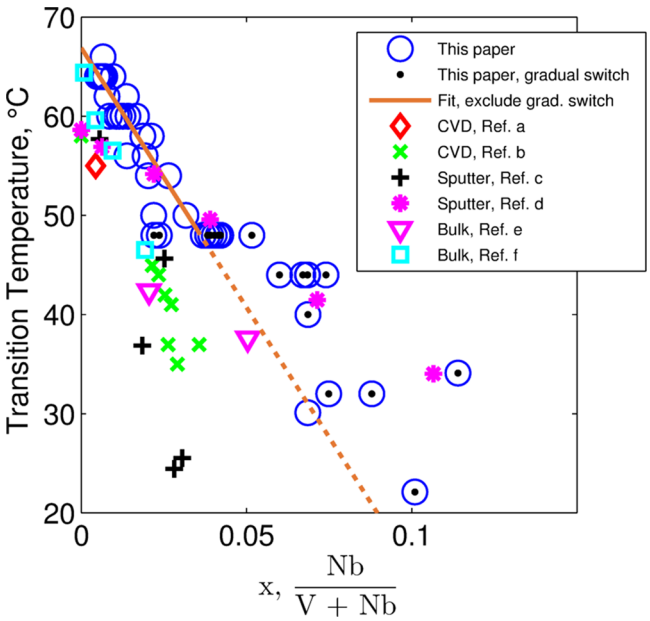

Figure 8. Temperature of the thermochromic transition as a function of Nb content in a $V_{1-x}Nb_xO_2$ combinatorial library. The linear fit at low Nb contents is extrapolated to higher Nb contents with a broken line. Transition temperatures from the literature for Nb-substituted VO_2 are included for comparison. Ref a is ref 21; ref b is ref 22; ref c is ref 16; ref d is ref 39; ref e is ref 51; ref f is ref 53.

that experienced at least a 30% increase in reflectance across the transition. Consistent with Figure 6 and 7 results, transition temperatures decreased with increasing Nb content, but there were no significant thermochromic transitions observed for regions of the film with Nb content greater than $x = 0.12$.

Results from the literature are also plotted in Figure 8 and indicate a higher dopant efficiency has often been found,[16,21,22,39] though there has been significant variation among studies and within some studies. The studies differed in their material preparation techniques, material composition measurements, and identification of the transition temperature, and several report transition temperatures for undoped VO_2 of less than 60 °C. The greater efficiency of Nb reported in these studies, however, may indicate that a greater fraction of the Nb was effective, for example, by acting as a substitutional impurity on the VO_2 lattice instead of segregating to a grain boundary or a point defect off the lattice. It is interesting also that there has been only one report of a transition temperature less than 30 °C.[16] Many studies report a minimum transition temperature between 35 and 50 °C,[22,39,51,53] suggesting that Nb may not be an efficient route to transition temperatures at Earth ambient temperatures.

The phase transition temperature in cation-doped VO_2 is often found to be depressed at a linear rate with dopant concentration at low concentrations, such as in ref 39 for Nb-substituted VO_2. In Figure 8, a linear fit was made to regions of the film with at least a 30% increase in reflectance and a sufficiently sharp transition, defined by a maximum rate of change in the reflectance dR/dT of at least 0.015 K^{-1}. The second of these requirements excluded regions of the library with transitions similar to that of 8.8% Nb in Figure 6; these regions are labeled "gradual switch" in Figure 8 figure legend.

According to this linear fit, the Nb substitution effected a transition temperature depression of 5.2 ± 0.7 °C/atomic percent Nb. The fit also indicates a transition temperature for pure VO_2 ($x = 0$) of 66.9 ± 2.0 °C, in keeping with our own measurements and the known value.[12−14,50] However, the majority of these transitions occurred at low Nb contents, $x <$ 0.04, and so represented transition temperatures greater than 50 °C. Further depression of the transition temperature occurred at higher Nb contents, but at lower efficiency with increasing Nb. Where the extrapolation of the linear fit from the low Nb content data would suggest that a transition temperature of 30 ± 2 °C at a Nb content of 0.07, our experimental results indicate that Nb contents of $x = 0.07$ result in a transition temperature of 44 °C and that much more Nb, up to $x = 0.1$, is necessary for a transition temperature of about 30 °C. Hence, at higher Nb contents, a lower fraction of the Nb contributed to depressing the transition temperature, or was otherwise less effective at doing so. The saturation of transition temperature depression at higher impurity levels has also been observed in materials of the $V_{1-x}W_xO_2$ composition.[23]

For thermochromic window applications, a composition with an appropriate transition temperature was found at greater than 8% Nb substitution. However, that the full transition for this composition occurred gradually over a 30 °C range (see Figure 6), and so would not fully occur within a single day at Earth ambient temperatures. Further, the difference between reflectances in the high temperature state and the low temperature state was decreased compared to lower Nb content films. For smart window applications, it may be better to take advantage of the elevated temperature between the glass window panes. On a hot sunny day, the temperature between glass panes can be elevated to 45 °C or greater,[5,8] which may allow a full transformation to occur or decrease in the necessary Nb dopant level. Alternatively, a more efficient dopant, such as tungsten, may be used.[18,19,23,56]

CONCLUSIONS

We describe the high-throughput characterization of thermochromic behavior in a Nb-substituted VO_2 thin film library. The library oxide film was prepared with a continuous concentration gradient with the cation varying from less than 1% Nb up to

dx.doi.org/10.1021/co500064p | ACS Comb. Sci. 2014, 16, 526−534

40% Nb across the 76.2 mm diameter wafer. Thermochromism was characterized in a custom-built NIR reflectance measurement apparatus, employing a high-throughput protocol both for data collection and analysis. Using this system, 165 unique film compositions can be measured in 14 hours with 4 °C temperature resolution (step size). Post-mortem analysis to reduce the thousands of resulting spectra to characteristic transition temperatures was automated in a separate script and occurred in minutes.

Across 80% of the library surface, a solid solution of $V_{1-x}Nb_xO_2$ in the VO_2 crystalline structure was found. Regions of the crystalline phase field with less than 15% Nb exhibit a NIR thermochromic transition from a low temperature phase of low NIR reflectance to a high temperature phase of high NIR reflectance. With increasing Nb content, the thermochromic transition temperature was depressed at an efficiency of (5.2 ± 0.7) °C/atomic percent Nb, and transition temperatures appropriate for thermochromic smart windows (35 °C) were found at Nb contents of greater than 8%. However, the high Nb content also resulted in a gradual transition occurring over a 30 °C temperature range and a decreased difference between the high and low temperature reflectances.

■ ASSOCIATED CONTENT

Ⓦ Web-Enhanced Feature

An animation of the NIR reflectance at all 35 temperatures probed on the $V_{1-x}Nb_xO_2$ combinatorial library is available as a multimedia enhancement of Figure 5 in the HTML version of the paper.

■ AUTHOR INFORMATION

Corresponding Author

*E-mail: sara.barron@nist.gov.

Author Contributions

The manuscript was written through contributions of all authors. All authors have given approval to the final version of the manuscript.

Notes

Certain commercial equipment, instruments, or materials are identified in this document. Such identification does not imply recommendation or endorsement by the National Institute of Standards and Technology, nor does it imply that the products identified are necessarily the best available for the purposes.
The authors declare no competing financial interest.

■ ACKNOWLEDGMENTS

The authors gratefully acknowledge Nhan Nguyen for measurements of the refractive index of VO_2, Ratan Debnath for the Au thin film, and Chris Amigo for support in apparatus assembly. The colormaps used in drawing some figures are available from ref 57. S.C.B. is grateful for financial support from an American Reinvestment and Recovery Act (ARRA) grant, administered through the University of Maryland.

■ REFERENCES

(1) *2011 Buildings Energy Data Book*; U.S. Department of Energy, Office of Energy Efficiency and Renewable Energy: Washington, DC, 2012.
(2) Selkowitz, S.; Lee, E. S. Advanced Fenestration Systems for Improved Daylight Performance. *Daylighting 98 Conf.* **1998**, No. LBNL-41461.
(3) Lee, E. S.; DiBartolomeo, D. L.; Selkowitz, S. E. Daylighting Control Performance of a Thin-Film Ceramic Electrochromic Window: Field Study Results. *Energy Build.* **2006**, *38*, 30−44.
(4) Lampert, C. M. Large-Area Smart Glass and Integrated Photovoltaics. *Sol. Energy Mater. Sol. Cells* **2003**, *76*, 489−499.
(5) Nilsson, A. M.; Roos, A. Evaluation of Optical and Thermal Properties of Coatings for Energy Efficient Windows. *Thin Solid Films* **2009**, *517*, 3173−3177.
(6) Saeli, M.; Piccirillo, C.; Parkin, I. P.; Binions, R.; Ridley, I. Energy Modelling Studies of Thermochromic Glazing. *Energy Build.* **2010**, *42*, 1666−1673.
(7) Hoffmann, S.; Lee, E. S.; Clavero, C. Examination of the Technical Potential of Near-Infrared Switching Thermochromic Windows for Commercial Building Applications. *Sol. Energy Mater. Sol. Cells* **2014**, *123*, 65−80.
(8) Baetens, R.; Jelle, B. P.; Gustavsen, A. Properties, Requirements, and Possibilities of Smart Windows for Dynamic Daylight and Solar Energy Control in Buildings: A State-of-the-Art Review. *Sol. Energy Mater. Sol. Cells* **2010**, *94*, 87−105.
(9) Barker, A. S.; Verleur, H. W.; Guggenheim, H. J. Infrared Optical Properties of Vanadium Dioxide Above and Below the Transition Temperature. *Phys. Rev. Lett.* **1966**, *17*, 1286−1289.
(10) Babulanam, S. M.; Eriksson, T. S.; Niklasson, G. A.; Granqvist, C. G. Thermochromic VO_2 Films for Energy-Efficient Windows. *Sol. Energy Mater.* **1987**, *16*, 347−363.
(11) Kim, H.; Kim, Y.; Kim, K. S.; Jeong, H. Y.; Jang, A.-R.; Han, S. H.; Yoon, D. H.; Suh, K. S.; Shin, H. S.; Kim, T.; Yang, W. S. Flexible Thermochromic Window Based on Hybridized VO_2/Graphene. *ACS Nano* **2013**, *7*, 5769−5776.
(12) Morin, F. J. Oxides Which Show a Metal-to-Insulator Transition at the Neel Temperature. *Phys. Rev. Lett.* **1959**, *3*, 34−36.
(13) Goodenough, J. B. The Two Components of the Crystallographic Transition in VO_2. *J. Solid State Chem.* **1971**, *3*, 490−500.
(14) Zylbersztejn, A.; Mott, N. F. Metal-Insulator Transition in Vanadium Dioxide. *Phys. Rev. B* **1975**, *11*, 4383−4395.
(15) Cavalleri, A.; Dekorsy, T.; Chong, H. H. W.; Kieffer, J. C.; Schoenlein, R. W. Evidence for a Structurally-Driven Insulator-to-Metal Transition in VO_2: A View from the Ultrafast Timescale. *Phys. Rev. B* **2004**, *70*, 161102.
(16) Jorgenson, G. V.; Lee, J. C. Doped Vanadium Oxide for Optical Switching Films. *Sol. Energy Mater.* **1986**, *14*, 205−214.
(17) Rakotoniaina, J. C.; Mokrani-Tamellin, R.; Gavarri, J. R.; Vacquier, G.; Casalot, A.; Calvarin, G. The Thermochromic Vanadium Dioxide: I. Role of Stresses and Substitution on Switching Properties. *J. Solid State Chem.* **1993**, *103*, 81−94.
(18) Sobhan, M. A.; Kivaisi, R. T.; Stjerna, B.; Granqvist, C. G. Thermochromism of Sputter Deposited $W_xV_{1-x}O_2$ Films. *Sol. Energy Mater. Sol. Cells* **1996**, *44*, 451−455.
(19) Jin, P.; Nakao, S.; Tanemura, S. Tungsten Doping into Vanadium Dioxide Thermochromic Films by High-Energy Ion Implantation and Thermal Annealing. *Thin Solid Films* **1998**, *324*, 151−158.
(20) Soltani, M.; Chaker, M.; Haddad, E.; Kruzelecky, R. V.; Margot, J. Effects of Ti−W Codoping on the Optical and Electrical Switching of Vanadium Dioxide Thin Films Grown by a Reactive Pulsed Laser Deposition. *Appl. Phys. Lett.* **2004**, *85*, 1958−1960.
(21) Manning, T. D.; Parkin, I. P.; Blackman, C.; Qureshi, U. APCVD of Thermochromic Vanadium Dioxide Thin Films—Solid Solutions $V_{2-x}M_xO_2$ (M = Mo, Nb) or Composites VO_2: SnO_2. *J. Mater. Chem.* **2005**, *15*, 4560.
(22) Piccirillo, C.; Binions, R.; Parkin, I. P. Nb-Doped VO_2 Thin Films Prepared by Aerosol-Assisted Chemical Vapour Deposition. *Eur. J. Inorg. Chem.* **2007**, *2007*, 4050−4055.
(23) Whittaker, L.; Wu, T.-L.; Patridge, C. J.; Sambandamurthy, G.; Banerjee, S. Distinctive Finite Size Effects on the Phase Diagram and Metal−Insulator Transitions of Tungsten-Doped Vanadium(IV) Oxide. *J. Mater. Chem.* **2011**, *21*, 5580−5592.
(24) Li, S.-Y.; Namura, K.; Suzuki, M.; Niklasson, G. A.; Granqvist, C. G. Thermochromic VO_2 Nanorods Made by Sputter Deposition:

Growth Conditions and Optical Modeling. *J. Appl. Phys.* **2013**, *114*, No. 033516.
(25) Li, S.-Y.; Niklasson, G. A.; Granqvist, C. G. Thermochromic Undoped and Mg-Doped VO_2 Thin Films and Nanoparticles: Optical Properties and Performance Limits for Energy Efficient Windows. *J. Appl. Phys.* **2014**, *115*, No. 053513.
(26) Hanak, J. J. The "Multiple-Sample Concept" in Materials Research: Synthesis, Compositional Analysis, and Testing of Entire Multicomponent Systems. *J. Mater. Sci.* **1970**, *5*, 964−971.
(27) Hanak, J. J.; Lehmann, H. W.; Wehner, R. K. Calculation of Deposition Profiles and Compositional Analysis of Cosputtered Films. *J. Appl. Phys.* **1972**, *43*, 1666−1673.
(28) Sawatzky, E.; Kay, E. Cation Deficiencies in RF Sputtered Gadolinium Iron Garnet Films. *IBM J. Res. Dev.* **1969**, *13*, 696−702.
(29) Fukumura, T.; Ohtani, M.; Kawasaki, M.; Okimoto, Y.; Kageyama, T.; Koida, T.; Hasegawa, T.; Tokura, Y.; Koinuma, H. Rapid Construction of a Phase Diagram of Doped Mott Insulators with a Composition-Spread Approach. *Appl. Phys. Lett.* **2000**, *77*, 3426−3428.
(30) Christen, H. M.; Silliman, S. D.; Harshavardhan, K. S. Continuous Compositional-Spread Technique Based on Pulsed-Laser Deposition and Applied to the Growth of Epitaxial Films. *Rev. Sci. Instrum.* **2001**, *72*, 2673−2678.
(31) Perkins, J.; del Cueto, J.; Alleman, J.; Warmsingh, C.; Keyes, B.; Gedvilas, L.; Parilla, P.; To, B.; Readey, D.; Ginley, D. Combinatorial Studies of Zn−Al−O and Zn−Sn−O Transparent Conducting Oxide Thin Films. *Thin Solid Films* **2002**, *411*, 152−160.
(32) Koinuma, H.; Takeuchi, I. Combinatorial Solid-State Chemistry of Inorganic Materials. *Nat. Mater.* **2004**, *3*, 429−438.
(33) Van Dover, R. B.; Schneemeyer, L. F. The Codeposited Composition Spread Approach to High-Throughput Discovery/Exploration of Inorganic Materials. *Macromol. Rapid Commun.* **2004**, *25*, 150−157.
(34) Green, M. L.; Takeuchi, I.; Hattrick-Simpers, J. R. Applications of High Throughput (Combinatorial) Methodologies to Electronic, Magnetic, Optical, and Energy-Related Materials. *J. Appl. Phys.* **2013**, *113*, No. 231101.
(35) Wilkinson, M.; Kafizas, A.; Bawaked, S. M.; Obaid, A. Y.; Al-Thabaiti, S. A.; Basahel, S. N.; Carmalt, C. J.; Parkin, I. P. Combinatorial Atmospheric Pressure Chemical Vapor Deposition of Graded TiO_2−VO_2 Mixed-Phase Composites and Their Dual Functional Property as Self-Cleaning and Photochromic Window Coatings. *ACS Comb. Sci.* **2013**, *15*, 309−319.
(36) Fujino, S.; Murakami, M.; Anbusathaiah, V.; Lim, S.-H.; Nagarajan, V.; Fennie, C. J.; Wuttig, M.; Salamanca-Riba, L.; Takeuchi, I. Combinatorial Discovery of a Lead-Free Morphotropic Phase Boundary in a Thin-Film Piezoelectric Perovskite. *Appl. Phys. Lett.* **2008**, *92*, No. 202904.
(37) Zarnetta, R.; Takahashi, R.; Young, M. L.; Savan, A.; Furuya, Y.; Thienhaus, S.; Maaß, B.; Rahim, M.; Frenzel, J.; Brunken, H.; Chu, Y. S.; Srivastava, V.; James, R. D.; Takeuchi, I.; Eggeler, G.; Ludwig, A. Identification of Quaternary Shape Memory Alloys with Near-Zero Thermal Hysteresis and Unprecedented Functional Stability. *Adv. Funct. Mater.* **2010**, *20*, 1917−1923.
(38) Takahashi, I.; Hibino, M.; Kudo, T. Thermochromic Properties of Double-Doped VO_2 Thin Films Prepared by a Wet Coating Method Using Polyvanadate-Based Sols Containing W and Mo or W and Ti. *Jpn. J. Appl. Phys.* **2001**, *40*, 1391−1395.
(39) Batista, C.; Ribeiro, R. M.; Teixeira, V. Synthesis and Characterization of VO_2-Based Thermochromic Thin Films for Energy-Efficient Windows. *Nanoscale Res. Lett.* **2011**, *6*, 1−7.
(40) Bassim, N. D.; Schenck, P. K.; Donev, E. U.; Heilweil, E. J.; Cockayne, E.; Green, M. L.; Feldman, L. C. Effects of Temperature and Oxygen Pressure on Binary Oxide Growth Using Aperture-Controlled Combinatorial Pulsed-Laser Deposition. *Appl. Surf. Sci.* **2007**, *254*, 785−788.
(41) Bassim, N. D.; Schenck, P. K.; Otani, M.; Oguchi, H. Model, Prediction, and Experimental Verification of Composition and Thickness in Continuous Spread Thin Film Combinatorial Libraries Grown by Pulsed Laser Deposition. *Rev. Sci. Instrum.* **2007**, *78*, 072203−072203−7.
(42) Schenck, P. K.; Bassim, N. D.; Otani, M.; Oguchi, H.; Green, M. L. Design and Spectroscopic Reflectometry Characterization of Pulsed Laser Deposition Combinatorial Libraries. *Appl. Surf. Sci.* **2007**, *254*, 781−784.
(43) Barron, S. C.; Gorham, J. M.; Green, M. L. Thermochromic Phase Transitions in VO_2-Based Thin Films for Energy-Saving Applications. *ECS Trans.* **2014**, *61*, 387−393.
(44) Zhang, Z.; Gao, Y.; Chen, Z.; Du, J.; Cao, C.; Kang, L.; Luo, H. Thermochromic VO_2 Thin Films: Solution-Based Processing, Improved Optical Properties, and Lowered Phase Transformation Temperature. *Langmuir* **2010**, *26*, 10738−10744.
(45) G03 Committee. *G173−03 Tables for Reference Solar Spectral Irradiances: Direct Normal and Hemispherical on 37 Tilted Surface*; ASTM International: West Conshohocken, PA, 2012.
(46) Rubin, M. Optical Properties of Soda Lime Silica Glasses. *Sol. Energy Mater.* **1985**, *12*, 275−288.
(47) Silversmit, G.; Depla, D.; Poelman, H.; Marin, G. B.; De Gryse, R. Determination of the V2p XPS Binding Energies for Different Vanadium Oxidation States (V^{5+} to V^{0+}). *J. Electron Spectrosc. Relat. Phenom.* **2004**, *135*, 167−175.
(48) Grundner, M.; Halbritter, J. XPS and AES Studies on Oxide Growth and Oxide Coatings on Niobium. *J. Appl. Phys.* **2008**, *51*, 397−405.
(49) Rüdorff, W.; Märklin, J. Untersuchungen an Ternären Oxiden Der Übergangsmetalle. III. Die Rutilphase $(V_{1-x}Nb_x)O_2$. *Z. Für Anorg. Allg. Chem.* **1964**, *334*, 142−149.
(50) Nag, J.; Haglund, R. F., Jr Synthesis of Vanadium Dioxide Thin Films and Nanoparticles. *J. Phys.: Condens. Matter* **2008**, *20*, No. 264016.
(51) Rao, C. N. R.; Natarajan, M.; Subba Rao, G. V.; Loehman, R. E. Phase Transitions and Conductivity Anomalies in Solid Solutions of VO_2 with TiO_2, NbO_2, and MoO_2. *J. Phys. Chem. Solids* **1971**, *32*, 1147−1150.
(52) Chae, B.-G.; Kim, H.-T.; Yun, S.-J.; Kim, B.-J.; Lee, Y.-W.; Kang, K.-Y. Comparative Analysis of VO_2 Thin Films Prepared on Sapphire and SiO_2/Si Substrates by the Sol−Gel Process. *Jpn. J. Appl. Phys.* **2007**, *46*, 738−743.
(53) Villeneuve, G.; Bordet, A.; Casalot, A.; Pouget, J. P.; Launois, H.; Lederer, P. Contribution to the Study of the Metal−Insulator Transition in the $V_{1-x}Nb_xO_2$ System: I—Crystallographic and Transport Properties. *J. Phys. Chem. Solids* **1972**, *33*, 1953−1959.
(54) MacChesney, J. B.; Guggenheim, H. J. Growth and Electrical Properties of Vanadium Dioxide Single Crystals Containing Selected Impurity Ions. *J. Phys. Chem. Solids* **1969**, *30*, 225−234.
(55) Jorgenson, G. *Electrochromic and Thermochromic Materials for Solar Applications with Emphasis on Niobium and Vanadium Oxides*; Lawrence Berkeley Laboratory: Berkeley, CA, 1984; Document LBL-18299.
(56) Takahashi, I.; Hibino, M.; Kudo, T. Thermochromic $V_{1-x}W_xO_2$ Thin Films Prepared by Wet Coating Using Polyvanadate Solutions. *Jpn. J. Appl. Phys.* **1996**, *35*, L438−L440.
(57) Geissbuehler, M.; Lasser, T. How to Display Data by Color Schemes Compatible with Red−Green Color Perception Deficiencies. *Opt. Express* **2013**, *21*, 9862−9874.